


Proteasome inhibition alters mitotic progression through the upregulation of centromeric α -Satellite RNAs

Rodrigo E. Cáceres-Gutiérrez¹, Marco A. Andonegui¹, Diego A. Oliva-Rico¹, Rodrigo González-Barrios¹, Fernando Luna¹, Cristian Arriaga-Canon¹, Alejandro López-Saavedra¹, Diddier Prada^{1,2}, Clementina Castro¹, Laurent Parmentier¹, José Díaz-Chávez¹, Yair Alfaro-Mora¹, Erick I. Navarro-Delgado¹, Eunice Fabian-Morales¹, Bao Tran³, Jyoti Shetty³, Yongmei Zhao³, Nicolas Alcaraz^{4,5}, Carlos De la Rosa⁶, José L. Reyes⁶, Sabine Hédouin^{7,*}, Florent Hubé⁷, Claire Francastel⁷ and Luis A. Herrera^{1,8} 

1 Instituto Nacional de Cancerología-Instituto de Investigaciones Biomédicas, UNAM, Unidad de Investigación Biomédica en Cáncer, Mexico City, Mexico

2 Departamento de Informática Biomédica, Faculty of Medicine, UNAM, Universidad Nacional Autónoma de México, Mexico City, Mexico

3 NCI CCR Sequencing Facility, Frederick National Laboratory for Cancer Research, MD, USA

4 The Bioinformatics Centre, University of Copenhagen, Copenhagen, Denmark

5 National Institute of Genomic Medicine, Mexico City, Mexico

6 Departamento de Biología Molecular de Plantas, Instituto de Biotecnología, Universidad Nacional Autónoma de México, Cuernavaca, Mexico

7 Epigenetics and Cell Fate, CNRS UMR7216, Université de Paris, Paris, France

8 Dirección General, Instituto Nacional de Medicina Genómica, Mexico City, Mexico

Keywords

26S proteasome; centromere; mitosis; ncRNA; α -Satellite

Correspondence

L. A. Herrera, Instituto Nacional de Cancerología-Instituto de Investigaciones Biomédicas, UNAM, Unidad de Investigación Biomédica en Cáncer, 14080 Mexico City, Mexico
Tel: +52 5553501901
Email: herreram@biomedicas.unam.mx

*Present address

Basic Sciences Division, Fred Hutchinson Cancer Research, Seattle, WA, USA

(Received 19 September 2019, revised 19 September 2021, accepted 3 November 2021)

doi:10.1111/febs.16261

Cell cycle progression requires control of the abundance of several proteins and RNAs over space and time to properly transit from one phase to the next and to ensure faithful genomic inheritance in daughter cells. The proteasome, the main protein degradation system of the cell, facilitates the establishment of a proteome specific to each phase of the cell cycle. Its activity also strongly influences transcription. Here, we detected the upregulation of repetitive RNAs upon proteasome inhibition in human cancer cells using RNA-seq. The effect of proteasome inhibition on centromeres was remarkable, especially on α -Satellite RNAs. We showed that α -Satellite RNAs fluctuate along the cell cycle and interact with members of the cohesin ring, suggesting that these transcripts may take part in the regulation of mitotic progression. Next, we forced exogenous overexpression and used gapmer oligonucleotide targeting to demonstrate that α -Sat RNAs have regulatory roles in mitosis. Finally, we explored the transcriptional regulation of α -Satellite DNA. Through *in silico* analyses, we detected the presence of CCAAT transcription factor-binding motifs within α -Satellite centromeric arrays. Using high-resolution three-dimensional immuno-FISH and ChIP-qPCR, we showed an association between the α -Satellite upregulation and the recruitment of the transcription factor NFY-A to the centromere upon MG132-induced proteasome inhibition. Together, our results show that the proteasome controls α -Satellite RNAs associated with the regulation of mitosis.

Abbreviations

APC/C, anaphase promoting complex/cyclosome; ASO, antisense oligonucleotide; ChIP, chromatin immunoprecipitation; CPC, chromosomal passenger complex; GO, gene ontology; H3S10ph, histone 3 phosphorylated on serine 10; SAC, spindle assembly complex; TF, transcription factor; TSS, transcription start site; α -Sat, α -Satellite.

Introduction

Most biological processes required to orchestrate healthy development and maintain tissue homeostasis in mammals rely on faithful expression of genetic programs. A wide range of mechanisms devoted to the regulation of these expression programs operate not only at the level of translation and transcription, through transcriptional or epigenetic mechanisms, but also at the level of the transcripts and the proteins themselves, controlling for their stability, subcellular localization, and function. In that respect, the proteasome has been shown to participate in the regulation of gene expression programs through the monitoring of the abundance of transcriptional regulators associated with chromatin [1].

The proteasome is a multisubunit assembly of proteases that selectively degrades proteins flagged for destruction by the ubiquitin conjugation system [2]. In concert with the ubiquitin system, the proteasome controls cell cycle progression through timely degradation of specific targets [3,4]. For instance, in the metaphase-to-anaphase transition, this occurs in coordination with the anaphase promoting complex/cyclosome (APC/C), an E3 ubiquitin ligase essential for the onset of anaphase [4]. APC/C ubiquitylates, among other proteins, CYCLIN B as well as SECURIN, an inhibitor of a protease known as SEPARASE. SEPARASE is required for the cleavage of cohesin rings, allowing for the separation of sister chromatids. APC/C ubiquitylates its targets in metaphase once no faulty kinetochore–microtubule attachments are detected. Such proteins are then cleared by the 26S proteasome, paving the way for chromosome segregation [4]. Accordingly, failure in the ubiquitylation of APC/C targets or in proteasome function prevents metaphase-to-anaphase transition [5].

On the other hand, studies of the dynamics of proteasome localization revealed that the nuclear proteasome binds to chromatin in a cell cycle-dependent manner and dictates the timing of cell cycle progression [6]. The proteasome also contributes to gene regulatory networks through controlling the turnover of several transcription factors and regulating histone modifications, thereby contributing to modulate the efficiency with which genes are transcribed by RNA polymerase II (RNA pol II) [1,6]. Hence, the proteasome is a major guardian of cell homeostasis, and alterations to proteasome subunits or localization are hallmarks of pathological conditions like cancer.

Outside of genes, the proteasome has also been shown to occupy specialized chromosomal domains

like centromeric regions [7]. In most eukaryotic species studied to date, centromeric DNA consists of large arrays of repetitive elements, termed satellite repeats, which provide a platform for the assembly of the kinetochore, the protein complex involved in the attachment of chromosomes to the mitotic spindle [8,9]. In humans, the centromere of each chromosome is composed of tandem arrays of repeated α -Satellite (α -Sat) monomers (AT-rich \sim 171 nucleotides long repeat units) in a head-to-tail orientation over up to hundreds of kilobases [10]. Centromeres are surrounded by pericentromeric satellite repeats that form the bulk of constitutive heterochromatin. The DNA sequences and organization underlying centromeres are not conserved across species, despite the function of this region and the associated kinetochore being highly conserved [11]. Yet, their transcriptional competency in most species studied so far suggested functional relevance for centromeric transcription or transcripts in centromere function [8,11]. RNAs transcribed from centromeres, or transcription through centromeric repeats, were shown to participate in the recruitment of essential protein components of the centromere and kinetochore including CENP-A (the distinctive H3 variant that constitutes the platform for kinetochore assembly) and CENP-C [12–14]. Interestingly, the abundance of centromeric RNAs seems to be regulated during the cell cycle [13–16]. In the mouse, they peak in G2 where they have been involved in the timely recruitment of the chromosomal passenger complex (CPC) including AURORA B, INCENP, and SURVIVIN just before the onset of mitosis [15]. Furthermore, centromeric transcripts from different organisms have been shown to stimulate AURORA B kinase activity, which is crucial for proper chromosome segregation [15,17]. Likewise, in human cells, the levels of α -Sat repeats transcripts could fluctuate and peak in G2/M [16], although their associated proteins have not been identified in this system.

Consistent with a tight regulation of centromeric repeats transcription or levels of their transcripts being required for centromere integrity and function, the knockdown of centromeric transcripts has detrimental effects on mitosis [14]. Conversely, aberrant high levels of centromeric transcripts or unscheduled transcription of the repeats are hallmark of pathological conditions with impaired cell cycle progression or mitotic defects. This includes centromeric and pericentromeric satellites in cancer cells [18], pericentromeric Sat III in stress conditions [19], and mouse minor satellites upon DNA damage [20]. Accumulation of pericentromeric satellite repeats has also been observed upon inhibition of the proteasome [7].

Altogether, the localization of the proteasome at centromeres together with the cell cycle-regulated levels of centromeric transcripts suggested a direct, yet to be uncovered, link among proteasomal activity, satellite repeats transcription, and cell cycle progression, which would be lost in pathological contexts of reduced proteasome functions.

Here, we used RNA-seq to analyze the transcriptional consequences of proteasome inhibition. We detected a remarkable upregulation of α -Sat RNAs independent of the mitotic arrest imposed by proteasome inhibitors. We showed that α -Sat RNAs fluctuate along the cell cycle and interact with members of the cohesin ring, suggesting that these transcripts may take part in the regulation of mitotic progression. We demonstrated that the accumulation of α -Sat RNAs, either through proteasome inhibition or through exogenous overexpression, delays mitotic progression. Then, we demonstrated that the targeted destruction of these transcripts hampers the onset of mitosis.

We also identified binding sites for the sequence-specific transcription factor (TF) NFY within α -Sat monomers and demonstrated that NFY accumulates at α -Sat DNA repeats upon MG132 treatment, along with epigenetic modifications compatible with active transcription. Our data demonstrate a novel link between the proteasome and cell cycle progression, through the control of α -Sat transcription.

Results

Proteasome inhibitors MG132 and bortezomib alter the transcription of centromeric α -Satellite repeats

To establish a link among proteasomal activity, cell cycle progression, and the transcription of centromeric RNAs, we used HCT-116 cells synchronized in G2/M and treated for a short period (3 h) with the proteasome inhibitors MG132 or bortezomib (ps-341/Velcade™) to avoid indirect effects. We analyzed the transcriptional output of these cells by RNA-seq and observed that both treatments induced transcriptomic changes in coding and noncoding RNAs, including from repetitive elements, compared to untreated cells (Table 1). Interestingly, among the coding transcripts, gene ontology (GO) terms related to ncRNA processing, RNA pol II transcription factor activity in proximal promoters and enhancers, and methyltransferase activity were downregulated (Fig. S1A). These data confirmed that proteasome inhibition may alter the transcriptome directly through the stabilization of proteins related to transcriptional regulation, or indirectly,

Table 1. Classification of differentially expressed transcripts upon treatment with proteasome inhibitors. Async, asynchronous (control cells); Bort, Bortezomib; nc, noncoding, rep, repetitive.

Experimental condition	Coding up	Coding down	nc up	nc down	rep up	rep down
MG132 (G2) vs. Async.	893	529	225	353	13	3
Bort. (G2) vs. Async.	694	875	279	325	26	1

by affecting the expression of genes that code for transcriptional regulators.

With respect to the transcription of repetitive DNA, both MG132 and bortezomib significantly affected the expression of 16 and 27 repetitive element subfamilies, respectively, of which 11 were deregulated by both treatments (Fig. S1B). We plotted the distribution of these sequences to reveal their density along the genome. Interestingly, several chromosomes showed a high density of differentially expressed repeats in the centromere or its surroundings (Fig. 1A, entire dataset in Dataset S1).

Next, we assessed the abundance of specific repetitive RNA classes in the different conditions of our RNA-seq (Fig. 1B). Bortezomib had the strongest effect and substantially increased the transcription of all the repeat classes analyzed. Conversely, MG132 specifically upregulated satellite RNAs, while other repeat classes were unaffected. Among the class of satellite repeats, α -Sat were the most upregulated under both, MG132 and bortezomib, treatments (Fig. 1B, red dots). Intriguingly, and although α -Sat transcription was efficiently attenuated by the RNA pol II inhibitor α -amanitin, the satellite transcript class showed an important increase upon the simultaneous addition of MG132 and α -amanitin. From our RNA-seq, we also determined the abundance of two specific α -Sat sequences cloned by our group (CGSW2 and CGSW3, see *Vectors* in **Materials and methods**), across the different treatments used (Fig. S1C). We observed that CGSW3 was upregulated by MG132 and bortezomib, and its accumulation could be prevented by α -amanitin. Conversely, CGSW2 was only upregulated by MG132. To validate these findings, we analyzed the relative abundance of consensus α -Sat, CGSW3 (α -Sat that maps to chromosome 10), pericentromeric Sat II, Subtelomeric TERRA, and interspersed LINE-1 after MG132 and bortezomib treatment, by RT-qPCR (Fig. 1C). Interestingly, the global α -Sat RNAs and CGSW3 were the most upregulated transcripts among those tested, confirming our observations from the RNA-seq.

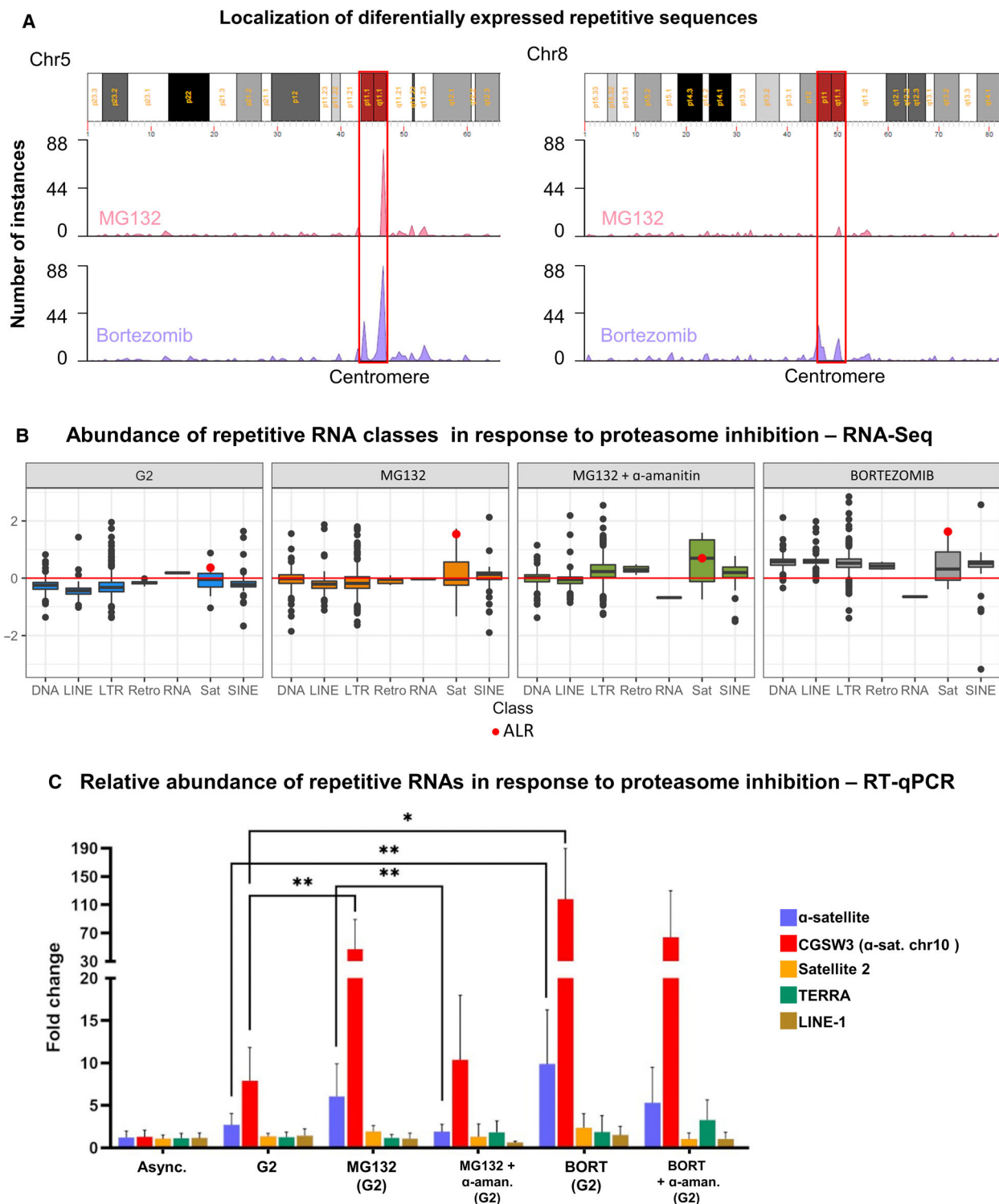


Fig. 1. Proteasome inhibition promotes derepression of centromeric repetitive sequences. A,B. RNA-seq analysis of HCT-116 cells synchronized in G2 and treated with 20 μ M MG132 or 100 nM bortezomib for 3 h. (A) Localization of differentially expressed repeat transcript subfamilies in MG132 (pink) and bortezomib (lavender). Instances are condensed in 500 kb windows. The entire dataset is available in Dataset S1. (B) log₂ fold change of different repeat classes compared to the control in RNA-seq (red dots indicate α -Sat RNA). (C) RNA abundance relative to U6 ($2^{-\Delta\Delta C_t}$ analysis) from RT-qPCR, for the indicated transcripts; error bars represent standard deviation. * $P < 0.05$, ** $P < 0.05$, and *** $P < 0.005$ according to a Wilcoxon signed rank test. The means of at least three independent experiments are shown.

Together, these findings showed that proteasome inhibition in HCT-116 cells alters the transcription of repetitive non-coding regions across the entire genome and has a major impact on the centromeric and pericentromeric repeats, key structures in the maintenance of genomic integrity.

α -Satellite upregulation upon proteasome inhibition is not a consequence of mitotic arrest

To gain insight into the regulation of α -Sat RNA abundance throughout the cell cycle, we synchronized HCT-116 cells in different phases of the cell cycle with a thymidine block followed by incubation for different lengths of time in fresh medium. We evaluated the cell cycle distribution, the mitotic index, and α -Sat RNA abundance in parallel (Fig. 2). Our synchronization method allowed us to enrich the G1, S, or G2/M population (Fig. 2A). Asynchronous cells, as well as cells in G1, S, or G2, had a mitotic index of <5% (Fig. 2B). Cells in G1 had no substantial enrichment in α -Sat RNAs, but cells in S-phase showed a 3.8-fold increase relative to the asynchronous control, and cells in G2 showed a 2.7-fold increase (Fig. 2C). We concluded that cell cycle progression through interphase is associated with changes in levels of α -Sat RNAs.

We then treated G2/M-enriched cultures with the spindle poisons nocodazole and taxol, and with MG132 or bortezomib. Taxol and nocodazole induce the activation of the spindle assembly checkpoint (SAC) through the alteration of microtubule dynamics. In turn, the SAC inhibits APC/C, resulting in mitotic arrest [4]. On the other hand, proteasome inhibitors act downstream of APC/C. These drugs prevent mitotic progression beyond metaphase by hindering the degradation of CYCLIN B and SECURIN, among other proteins [5].

Spindle poisons and proteasome inhibitors disturbed cell cycle progression with different efficiencies (Fig. 2A). While nocodazole had a mild effect on mitosis, taxol efficiently arrested cells in mitosis (Fig. 2B). However, these drugs had little or no effect on the abundance of α -Sat RNAs relative to control cells (Fig. 2C). Conversely, MG132 and bortezomib also induced a mild mitotic arrest (Fig. 2B) but promoted a strong enrichment in α -Sat RNAs levels (Fig. 2C). Hence, the upregulation of α -Sat RNAs upon MG132 or bortezomib treatment is the direct result of proteasome inhibition rather than of the enrichment in mitotic cells. Next, to assess whether proteasome inhibition could upregulate α -Sat RNAs in mitosis, we arrested cells in mitosis with taxol for 9 h and then

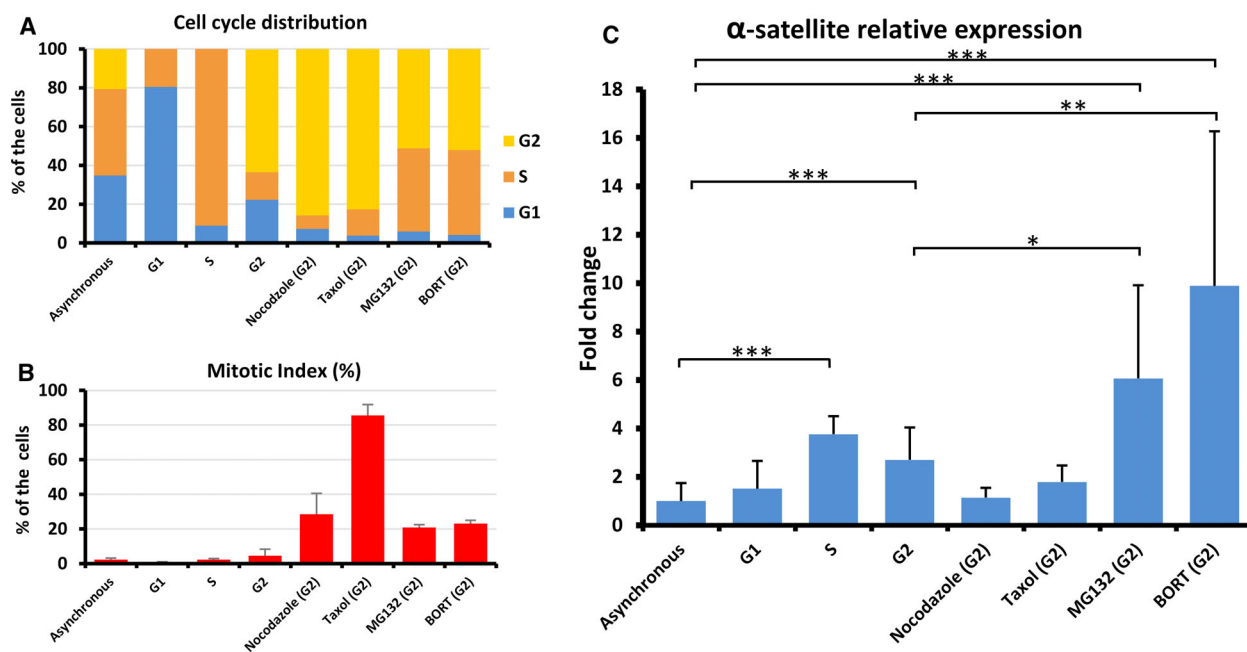


Fig. 2. α -Sat upregulation upon proteasome inhibition does not depend on mitotic arrest. (A) DNA content, indicative of cell cycle distribution, was determined by flow cytometry. (B) Mitotic index was determined with eosine/methylene blue staining. (C) U6-relative α -Sat RNA abundance in cells synchronized in different phases of the cell cycle. Cells treated with spindle poisons and proteasome inhibitors were synchronized in G2 beforehand. In A, B, and C, the means of at least three independent experiments are shown; error bars represent standard deviation. * P -value < 0.05, ** P -value < 0.01, and *** P -value < 0.001 according to a Wilcoxon analysis.

treated them with bortezomib for another 3 h. This treatment induced an increase in global α -Sat RNAs levels as well as in CGSW3 α -Sat RNA (Fig. S2A). Therefore, α -Sat RNA upregulation through proteasome inhibition can occur in mitotic cells.

Since indirect inhibition of APC/C through taxol or nocodazole treatment had no significant effect on α -Sat transcription, we reasoned that the regulation of this region is independent of APC/C. To test this, we directly inhibited the APC/C in G2/M-synchronized cells with its cell permeable and specific inhibitor pro-TAME [5] and evaluated α -Sat RNAs levels by RT-qPCR. We observed no significant difference in α -Sat RNAs abundance between pro-TAME-treated and control cells (Fig. S2B), showing that the proteasome regulates α -Sat transcription in an APC/C-independent manner.

α -Sat RNA abundance controls mitotic progression in cancer cells

To determine whether increased levels of α -Sat RNAs observed in HCT-116 cells could be involved in deregulated mitotic progression, we set out to identify proteins associated with these transcripts, using RNA pull-down assay (a depiction of the procedure is shown in Fig. S3A). We used *in vitro* transcribed RNAs from the CGSW2 sequence, consisting of five consecutive α -Sat repeats (Fig. S3B), and a control RNA of the same size from the luciferase cDNA. The proteins coprecipitated with α -Sat RNAs or with the control RNAs were identified by mass spectrometry. Because many proteins have intrinsic ability to bind RNA and proteins from large families with extensive sequence homology are difficult to link unambiguously to a single protein, we used very stringent criteria for data analysis. We focused on proteins precipitated exclusively with α -Sat RNA, with a number of unique peptides ≥ 5 , and we identified 28 α -Sat RNA-associated proteins (Table S1). Interestingly, 11 of these proteins are known to be enriched in centromeres [21]. Gene ontology, using Cellular Components track and analysis of protein networks [22], identified two small hubs: the nuclear cohesion complex, containing SMC1A, SMC3, and RAD21, whose dynamics is essential for proper chromosome segregation, and a hub centered on the splicing factor SF3B1, containing splicing factors and heterochromatin-associated chromatin remodelers (Fig. 3). Next, we used the catRAPID server to perform an *in silico* search for proteins from the human proteome with the ability to bind the CGSW2 RNA. Interestingly, 22 of the 28 proteins identified by our RNA pull-down assay were also predicted to bind

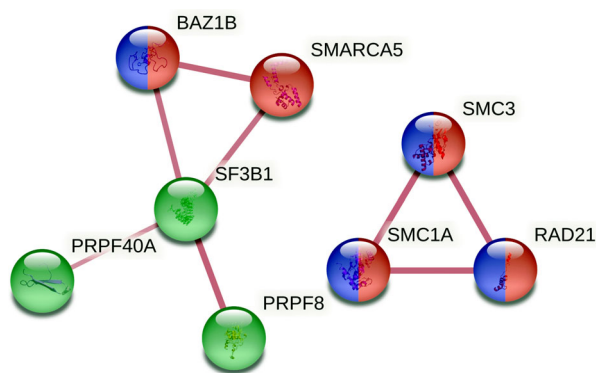


Fig. 3. α -Sat RNA-enriched proteins. The proteins obtained by the α -Sat RNA pull-down and identified by mass spectrometry were analyzed using the STRING software to detect interaction networks. These proteins are represented by nodes. Red nodes represent proteins that belong to the *condensed chromosome* ontology (cellular component). Blue nodes represent proteins that belong to the *chromosome, centromeric region* ontology (cellular component). Green nodes represent proteins that belong to the *spliceosome* ontology (cellular component). Edges represent physical protein-protein interactions.

CGSW2 by the catRAPID server [23] (Table S1). Table 2 reports the interaction propensity measurement for the proteins shown in Fig. 3. Remarkably, the cohesin ring component SMC1A shows a higher interaction propensity than the previously recognized RNA-binding and spliceosome components PRPF8 and SF3B1, underscoring the likelihood of its interaction with the CGSW2 RNA. These data suggested that α -Sat RNAs could participate in the regulation of mitotic progression through their interaction with cohesins.

Based on their interaction with key mitotic regulators, we then asked whether α -Sat RNAs could control mitotic progression. We first determined whether changes in α -Sat RNA levels induced by proteasome inhibitors altered the mitotic index of HCT-116 cell cultures. To this end, we treated G2-synchronized cells

Table 2. *In vitro*-determined interaction propensity of the proteins shown in Fig. 3 with the α -Sat sequence CGSW2.

Protein	Interaction propensity
SMARCA5	74.47
BAZ1B	72.41
PRPF40A	72.33
SMC1A	52.36
SF3B1	50.13
PRPF8	47.54
RAD21	N/A
SMC3	N/A

with MG132 or bortezomib with or without α -amanitin and analyzed histone 3 serine 10 phosphorylation (H3S10), a hallmark of mitotic chromosomes, by flow cytometry (Fig. 4A). As expected, proteasome inhibition with MG132 or bortezomib induced the accumulation of mitotic cells. Interestingly, this inhibition coincided with the accumulation of α -Sat RNAs since simultaneous treatment of MG132 or bortezomib with α -amanitin partially abolished both the accumulation of mitotic cells and the increase in α -Sat RNAs (Figs 4A and 1C). Nonetheless, statistically significant differences were only observed between bortezomib and bortezomib + α -amanitin for the percentage of H3S10ph-positive cells, and between MG132 and MG132 + α -amanitin for α -Sat abundance (Fig. 4A and 1C). Therefore, to specifically assess whether α -Sat RNA abundance could play a role in mitotic progression, we targeted these transcripts for degradation with LNA gapmer antisense oligonucleotides (ASOs) in HCT-116 cells (Fig. 4B,C). We transfected a mix of two different gapmers designed against the α -Sat consensus sequence and used mock transfection and a gapmer targeting LacZ for comparison. The cells were

either harvested after 24 h without any further treatment (Fig. 4B) or treated with nocodazole for 8 h, starting 16 h after the transfection, to enrich the mitotic population (Fig. 4C). Our targeting strategies reduced α -Sat RNAs to 37–44% (Fig. S4A,B). Interestingly, cultures transfected with ASOs targeting α -Sat RNAs showed a remarkable decrease in the mitotic index.

To confirm the relationship between α -Sat RNA abundance and mitosis, we set out to establish a forced expression model. First, we analyzed endogenous α -Sat RNA in sense and antisense orientation, by Northern blot, in a panel of epithelial cancer cell lines (Fig. S5A). We detected RNAs ≥ 10 kb, along with smaller transcripts of ~ 1 to ~ 9 kb, and two bands corresponding to the exact size of the ribosomal RNA 18S and 28S subunits. A stronger signal was observed for transcripts in the sense than in the antisense orientation [24]. This pattern was observed in all the cell lines tested, except for SW-480 cells, in which α -Sat RNA was undetectable. Next, we analyzed α -Sat transcripts in HEK293 neonatal foreskin keratinocytes (non-cancerous epithelial cells), peripheral blood leukocytes

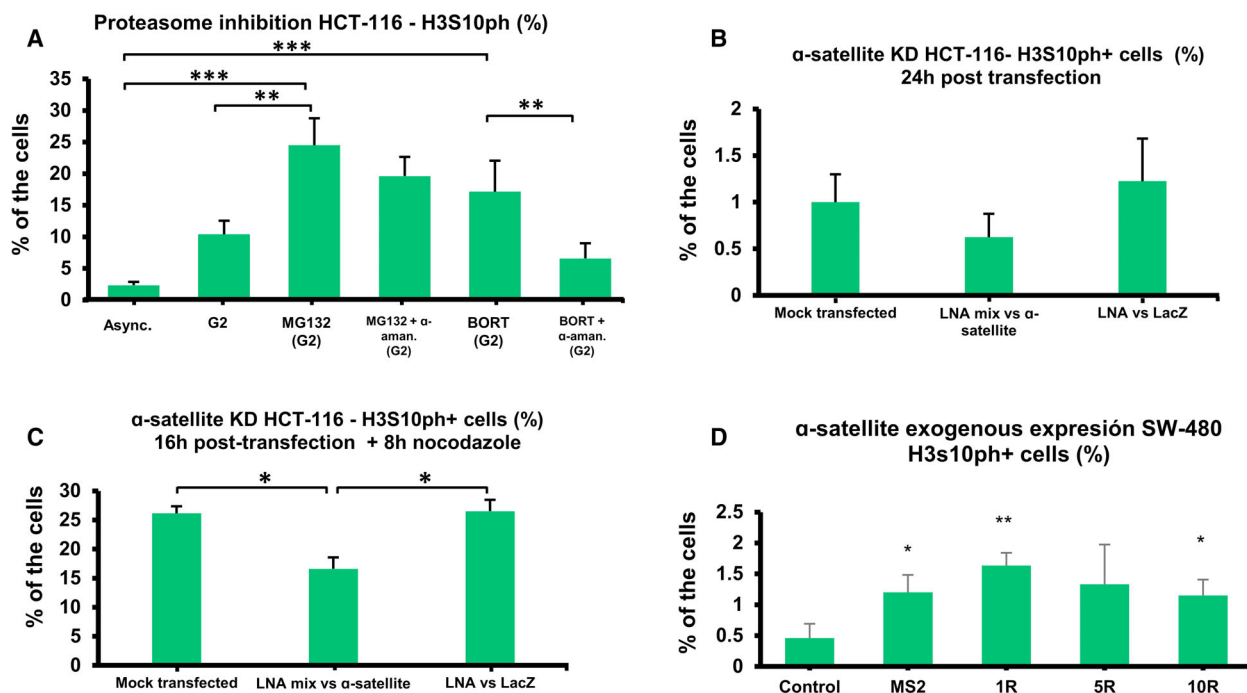


Fig. 4. α -Sat transcript levels control G2-M transition. (A) Mitotic index (H3S10ph-positive cells) of G2-synchronized HCT-116 cells treated with MG132/bortezomib with or without α -amanitin. * $P < 0.05$, ** $P < 0.01$, and *** $P < 0.001$ according to the χ^2 distribution. (B) Mitotic index of HCT-116 cells harvested 24 h after transfection with the indicated gapmer antisense oligos. (C) Mitotic index of HCT-116 cells treated with nocodazole $2 \mu\text{g mL}^{-1}$ for 8 h, starting 16 h after transfection with the indicated gapmer antisense oligos. * P -value ≤ 0.05 according to a Student's t test, with. In A–D, means of at least three independent experiments are shown, and error bars represent standard deviation. (D) Mitotic index of SW-480 cells transfected with plasmids bearing MS2, CGSW2, CGSW3, or CGSW10 under the control of a CMV promoter. Statistical analysis was performed with the Welch two-sample t -test; * $P < 0.05$, ** $P < 0.01$.

from three healthy donors, and BT20 breast cancer cells. While α -Sat RNA was undetectable in the non-cancerous epithelial cell line, we observed RNAs ≥ 10 kb in the noncancerous leukocytes and in BT20 cancer cells (Fig. S5B). Then, to determine whether endogenous α -Sat transcription could be induced in low expression cells, we treated asynchronous HEK293, SW-480, and HCT-116 (used as a positive control) cells with MG132 and bortezomib and measured α -Sat relative abundance by RT-qPCR (Fig. S5C). Interestingly, α -Sat transcription could be activated by both proteasome inhibitors in HEK293 cells but, in SW-480 cells, only a slight increase was detectable under bortezomib. Together, these data suggest that α -Sat arrays are transcriptionally repressed in SW-480 cells.

Based on our Northern blots and proteasome inhibition treatments, we decided to transfect SW-480 cells with different expression plasmids containing 1, 5, or 10 α -Sat repeats, or a construct containing 24 MS2 repeats from the MS2 phage (see *Vectors* in [Materials and methods](#)). Forty-eight hours after transfection, cells were harvested, and the mitotic index (Fig. 4D) and abundance of α -Sat RNAs (Fig. S4C) were determined. Interestingly, the highest effects on the mitotic index were observed in cells transfected with the 1 and 10 α -Sat monomer sequences (Fig. 4D, 1R and 10R). Transfection with MS2 phage RNA also significantly changed the accumulation of mitotic cells with respect to the control. However, this transcript accumulated much more efficiently in the cell than α -Sat RNAs; the maximum forced expression of α -Sat corresponded to 1.1 times the abundance of U6, while the maximum abundance of MS2 in MS2-transfected cells corresponded to 282 times the abundance of U6 (Fig. S4D). These data suggested that α -Sat RNAs alter mitotic progression in SW-480 cells and that milder mitotic delays can be induced by other repetitive RNAs. Together with our α -Sat RNA knockdown and the simultaneous inhibition of the proteasome and RNA pol II experiments, these findings demonstrate that α -Sat RNAs regulate mitotic progression.

α -Sat centromeric arrays contain TATA and CCAAT TF-binding motifs

Little is known about the transcriptional regulation of satellite DNA regions. These sequences are thought to be transcribed by the read through of upstream genes or transposable elements, but satellite DNA regions are punctuated by TF-binding motifs like the rest of the genome [10,25]. It is tempting to speculate that satellite transcription is driven by cryptic promoter-like regions. Using the α -Sat consensus [26] as query in the

NCBI BLAST tool [27], we retrieved 61 462 α -Sat monomers from the NCBI human nucleotide collection. Using the Morgan Hunter algorithm (code available as Appendix S1), these monomers were analyzed to detect sequences matching the position-specific frequency matrices (PSFM) of TATA [28,29], GC [28], and CCAAT boxes [30], three major TF-binding motifs found in many pol II promoters [28]. Remarkably, 9.71% of the individual α -Sat monomers analyzed bear at least one TATA box, and 4.25% bear a CCAAT box, while no GC boxes were detected. Then, we evaluated the score of the identified TF-binding motifs as previously described [31]. Unexpectedly, this analysis revealed that the scores for the CCAAT motifs found along α -Sat monomers in the 3'-5' orientation were higher than the scores of those in the 5'-3' orientation (Fig. 5A). Furthermore, the 3'-5' TF-binding motifs found on α -Sat monomers had higher mean scores than those of randomly selected human DNA clones or randomly generated AT-rich DNA. The scores of these 3'-5' sites were most similar to those of previously recognized CCAAT promoters, which indicated a high likelihood of TF binding.

Interestingly, we also observed that centromeric α -Sat arrays can bear TF-binding motifs within and between α -Sat monomers (Fig. S6A). A BLAT search revealed that 48 of 70 clones evaluated contained stretches of α -Sat repeats that mapped to the site of primary constriction of different human chromosomes [32] (Dataset S2).

Next, to gain insights into possible regulatory roles of CCAAT and TATA boxes within α -Sat arrays, we mapped the positive monomers (2780 and 5968, respectively) to the human genome, along with the location of α -Sat sequences that were upregulated upon proteasome inhibition in our RNA-seq (Fig. 5B, Dataset S3). Remarkably, α -Sat monomers bearing a CCAAT box partially overlapped with the α -Sat sequences upregulated upon proteasome inhibition, unlike α -Sat monomers bearing a TATA box. These results suggest a possible role for CCAAT boxes in α -Sat array upregulation upon proteasome inhibition.

Throughout the genome, CCAAT boxes are recognized and bound by NFY, a trimeric TF responsible for the G2-phase transcriptional increase in several genes essential for mitotic progression, including *CCNB2* (which codes for cyclin B) [33,34]. To determine whether NFY could associate with α -Sat repeats, we assessed the localization of its subunit NFY-A relative to kinetochores and α -Sat arrays by G2-synchronized cells treated with MG132 or bortezomib by using immuno-FISH for labeling and 3D-Structured Illumination Microscopy (3D-SIM) for

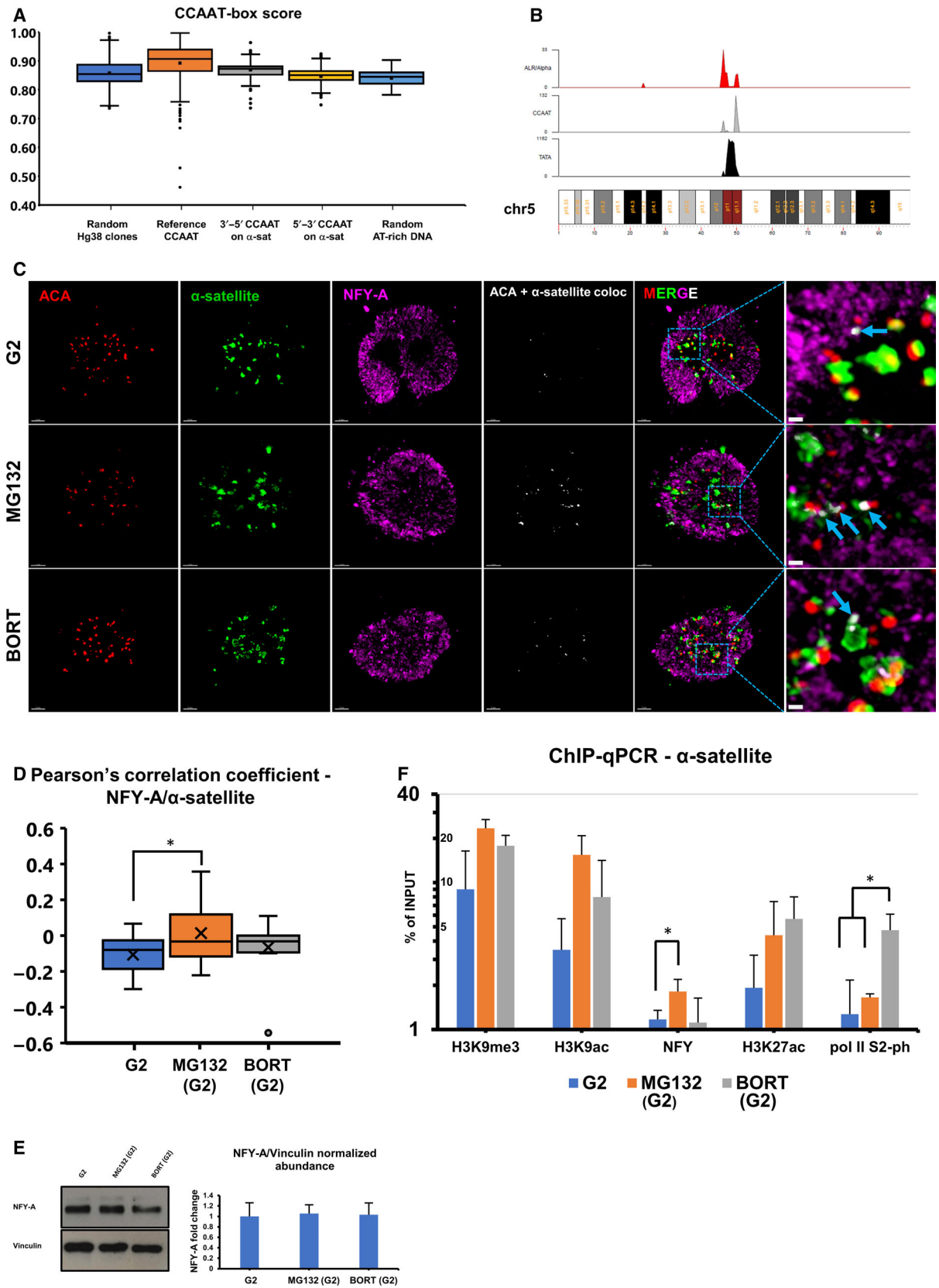


Fig. 5. CCAAT box and NFY occupancy at α -Sat repeats. (A) Scores of all the CCAAT motifs detected in randomly chosen Hg38 assembly BAC clones, a list of CCAAT/TATA-bearing promoters (reference [31]/reference [28] and the Eukaryotic Promoter Database (EPD) (reference [29])), CCAAT boxes found in the 3'-5' orientation on α -Sat monomers, CCAAT boxes found in the 5'-3' orientation on α -Sat monomers, and randomly generated DNA containing 63% AT. For the data in each graph, statistically significant differences between all groups were determined according to a Wilcoxon analysis (P -value $< 10^{-7}$). At least 433 scores were included in each group. (B) Location of CCAAT and TATA box-bearing α -Sat monomers (grey and black histograms, respectively) and the α -Sat RNAs differentially expressed in MG132 and bortezomib (red histogram). Portions of chromosomes 5 and 8 are shown (entire dataset available in Dataset S3). (C) NFY-A localization relative to the centromeres in HCT-116 cells. 3D reconstruction of structured illumination slices from Z-stack images (83 nm per slice) of NFY-A and ACA IF + α -Sat DNA FISH. The insets show the colocalization of α -Sat DNA with NFY-A (white). Scale bars in the insets represent 320 nm. (D) Pearson's correlation coefficient between the NFY-A and the α -Sat DNA signals from the immune-FISH experiments. Fifteen cells from three independent experiments were analyzed in each point. *: Statistically significant difference according to a one-tailed, paired Student's t test P -value < 0.025 . (E) Western blot showing the abundance of NFY-A in whole HCT-116 cell extracts. VINCULIN was used as a loading control. On the left, a blot representative of three independent experiments is shown, and on the right, a plot of the VINCULIN-normalized densitometric analysis of NFY-A abundance of the three experiments is shown. Error bars represent standard deviations. (F) IgG-normalized ChIP-qPCR of global α -Sat DNA in G2-synchronized and MG132 (G2)- or bortezomib (G2)-treated cells. Statistically significant differences were obtained with the Welch two-sample t -test. * P -value < 0.05 . The means of at least three independent experiments are shown; error bars represent standard deviations.

imaging (Fig. 5C). 3D-SIM imaging provides better resolution in terms of colocalization in multichannel imaging since lateral and axial resolution of traditional wide-field and confocal imaging techniques are no better than 200 and 600 nm, respectively, due to diffraction properties of the light, meaning they are unsuitable for determining the exact location or distribution of proteins. In contrast, lateral and axial resolution of 3D-SIM (100 and 300 nm respectively), along with imaging postprocessing, greatly enhance resolution, contrast and precision of colocalization over traditional wide-field and confocal imaging techniques. We measured Pearson's correlation coefficient between NFY-A and α -Sat probe staining in the 3D-SIM images (Fig. 5D). Although some foci of NFY-A and α -Sat colocalization were visible in untreated cells, negative Pearson's coefficients indicated that the marks are mutually exclusive. Nevertheless, colocalization foci were more frequent in MG132-treated cells (Fig. 5C), along with an increase in Pearson's correlation coefficient, suggesting that interactions may take place specifically under this condition (Fig. 5D). This was not the case in bortezomib-treated cells. We confirmed the specificity of our NFY-A antibody with shRNA against the NFY-A mRNA followed by IF staining of this protein (Fig. S6B,C). Moreover, we assessed NFY-A levels under MG132 and bortezomib treatment in western blot, but no changes were detectable (Fig. 5E). Therefore, the accumulation of NFY-A in centromeric regions under MG132 treatment was not due to a mere increase in its overall protein levels. We concluded that NFY-A is recruited to the centromere upon MG132 treatment.

Next, we performed ChIP experiments to confirm the NFY-A binding at α -Sat DNA upon MG132

treatment. We analyzed the enrichment of the histone post-translational modifications H3K9me3, H3K9ac, and H3K27ac to understand if changes in histone marks classically related to centromeric chromatin regulation and promoter/enhancer activity were involved in centromeric upregulation upon proteasome inhibition. We also determined the enrichment of RNA pol II phosphorylated on serine 2 (pol II-s2ph), a post-translational modification associated with transcriptional elongation. To assess the specificity of NFY-A occupancy and the mentioned histone marks on α -Sat arrays, we performed parallel ChIPs on Sat II DNA (which showed no significant transcriptional upregulation upon proteasome inhibition, as shown in Fig. 1C). A significant increase in the presence of NFY-A on α -Sat DNA was observed in MG132 treatment but not under bortezomib (Fig. 5F), consistent with our immuno-FISH results. A similar trend was observed with chromosome 4-specific α -Sat primers (Fig. S6D). The promoter of the *CCNB2* gene (which codes for cyclin B) from G2-synchronized cells was used as a positive control of NFY-A occupancy [33] (Fig. S6D). Conversely, no significant NFY-A presence was detected on Sat II repeats (Fig. S6E), consistent with the fact that Sat II RNAs are not upregulated upon proteasome inhibition.

MG132 and bortezomib induced different changes in epigenetic marks on α -Sat DNA (Fig. 5F). MG132 treatment induced a tendency toward an increase in H3K9ac and H3K27ac levels, while the accumulation of active RNA pol II was modest. Conversely, bortezomib was associated with slighter changes in H3K9ac but higher levels of active RNA pol II. Both, MG132 and bortezomib, promoted similar increases in H3K27ac and H3K9me3. On Sat II DNA, the patterns

of H3K9me3 and H3K9ac enrichment were similar to those of α -Sat DNA, but the H3K27ac and active RNA pol II epigenetic patterns differed between the α -Sat and Sat II DNA (compare Fig. 5F and Fig. S6D). The level of H3K27ac was qualitatively similar to that of active RNA pol II in both regions across treatments (compare H3K27ac to RNA pol II S2-ph in Fig. 5F and Fig. S6D). These results show that NFY enrichment in α -Sat DNA is clearly associated with α -Sat RNA upregulation in response to MG132, and that histone H3K9ac and H3K27ac could take part in the process.

Discussion

This is, to the best of our knowledge, the first report of the upregulation of centromeric α -Sat RNAs upon proteasome inhibition. This was observed in human cell lines after only 3 h of treatment with the proteasome inhibitors MG132 or bortezomib. Prior work in human cancer cells has reported that transcriptional deregulations induced by proteasome inhibition are strongly dependent on the kinetics used, with an increase in the number of genes differentially expressed by proteasome inhibition, as well as their fold change, over time in the presence of the inhibitors [35,36]. Yet, transcriptional changes observed after longer periods of treatment could be triggered by indirect effects caused by changes in cellular phenotypes. In contrast, the α -Sat upregulation that we reported is relatively rapid, suggesting that it is an early response of proteasome inhibition, unlikely to result from phenotypic changes that may affect cells upon such longer treatments. In our conditions, short-term treatment avoided, for instance, the onset of cohesion fatigue, a phenomenon observed in metaphase-arrested cells where sustained microtubule pulling forces break sister chromatid cohesion (e.g., upon proteasome inhibition), resulting in premature segregation, spindle assembly checkpoint activation, and eventually, cell death [37]. Thus, our observations underscore the involvement of the proteasome in the transcriptional regulation of centromeric α -Sat repeats.

Our data also contribute to understanding a chain of events leading to α -Sat upregulation. Proteasome inhibition has been previously associated with epigenetic alterations. Nevertheless, the epigenetic changes caused by proteasome inhibition on α -Sat DNA had not been assessed. In our experiments, proteasome inhibition was associated with an enrichment of H3K9ac, H3K9me3, and H3K27ac on α -Sat DNA. H3K9ac is associated with chromatin relaxation and active transcription, while H3K9me3 is related to

heterochromatin and transcriptional repression. In the centromeric chromatin context, the H3K9me3/H3K9ac ratio is known to regulate the H3/CENP-A nucleosome turnover [38]. Therefore, the interplay of the opposing roles of H3K9me3 and H3K9ac at centromeric regions is worth further analysis. Moreover, the association among H3K27ac, α -Sat DNA upregulation, and proteasome inhibition particularly drew our attention. H3K27ac is a known marker of enhancer/promoter activity whose global levels have been shown to increase in response to proteasome inhibition. In addition, short-term MG132 treatment (4 h) has been shown to cause an enrichment of H3K27ac at the transcription start site (TSS) of early upregulated genes [35]. Interestingly, this epigenetic mark was not associated with the TSS of genes upregulated after 24 h of proteasome inhibition. These observations suggest that, in response to proteasome inhibition, the previously discovered H3K27ac pulse could be responsible for the early α -Sat DNA upregulation. This hypothesis is in line with the regulatory elements that we found embedded in α -Sat DNA arrays. Indeed, we detected CCAAT boxes both between and within α -Sat arrays. Interestingly, the α -Sat monomers bearing such TF-binding motifs showed a remarkable colocalization with the areas of α -Sat upregulation in response to proteasome inhibition in our RNA-seq. Furthermore, we showed an enrichment of NFY-A at α -Sat DNA, without changes in its global protein levels, in response to MG132, but not under bortezomib. We also demonstrated that α -Sat upregulation was efficiently attenuated by α -amanitin in MG132 treatment, but not in bortezomib.

Recent work determined the contribution of the TF ZFAT to the regulation of centromeric transcription. This protein was demonstrated to increase the centromeric levels of the acetyltransferase KAT2B, which catalyzes H4K8 acetylation [39]. In turn, H4K8ac recruits the bromodomain-containing protein BRD4, which promotes RNA pol II progression through its interaction with the P-TEFb complex [39,40]. Similarly, NFY could play a role in epigenetic remodeling to allow α -Sat upregulation. In line with this view, this factor can bind condensed DNA and promote the formation of permissive chromatin [41]. Opposed to this hypothesis is the fact that NFY-A is not accumulated in α -Sat DNA arrays under bortezomib treatment, although this treatment also induced an important α -Sat overexpression. However, this can be explained by different mechanisms of action of these two drugs. Although we showed that these differences do not lie on NFY-A levels, other factors could be responsible

for them. Indeed, different proteasome inhibitors may prevent the destruction of distinct targets [42] and lead to distinct phenotypes. Furthermore, differences in the attenuation of α -Sat upregulation in MG132 and bortezomib by α -amanitin suggest transcription by distinct RNA polymerases, since RNA pol II is sensitive to α -amanitin and RNA pol I is not [43]. Moreover, the α -Sat upregulation we observed in response to MG132 and bortezomib could occur through distinct transcriptional activators that result in similar epigenetic modifications. Nonetheless, we failed to test NFY-A's functional role in α -Sat upregulation through its depletion since, consistent with previous reports [44], NFY-A knockdown seriously impaired the survival of HCT-116 and SW-480 cells in RNAi assays (data not shown). Therefore, novel experimental setups will be essential to interrogate these models.

α -Sat transcription level and the functions of the RNAs resulting from it are known to change along the phases of the cell cycle [10]. Our data showed high levels of α -Sat RNA in the S and G2 phases that decline to their lower level in G1. Similarly, recent research in human cells showed that α -Sat RNAs peaked in S/G2 were stable throughout mitosis, and decreased in G1 [16]. Thus, our results support previous findings on α -Sat RNAs oscillations along the cell cycle.

We also observed that proteasome inhibitors promote a higher α -Sat RNA increase in G2-synchronized cells than in asynchronous cells (compare Fig. 1C to Fig. S5C). Furthermore, we showed that proteasome inhibition can promote α -Sat RNA upregulation during mitosis and proved that neither the APC/C nor the SAC is responsible for regulating α -Sat transcription. α -Sat transcription in G2 is of special interest since, in addition to its own role, it defines the abundance α -Sat RNA at the onset of mitosis. In G2, it has been reported that α -Sat transcription from pericentromeres is associated with correct SUV39H1 localization, promoting correct heterochromatin maintenance, which is later required for proper chromosome segregation [45]. In mitosis, centromeric RNAs are known to stimulate Aurora B activity, which is essential for proper chromosome segregation [15,17]. Hence, we demonstrated that the proteasome has an important role in α -Sat regulation during G2/M and that its influence on the cell cycle is not limited to the ubiquitin-dependent degradation of proteins.

We reported an association between α -Sat RNA levels and mitotic progression. We detected an accumulation of mitotic cells associated with α -Sat upregulation in MG132 or bortezomib treatment. Both the mitotic delay and the α -Sat RNA increase could be attenuated by transcriptional inhibition. Concordantly,

exogenous α -Sat expression also perturbed mitotic progression, while the targeted destruction of α -Sat RNAs with gapmers hindered mitotic onset. Furthermore, we identified α -Sat-RNA-interacting proteins that belong to complexes involved in RNA splicing and pericentric heterochromatin but, most importantly, the members of the cohesin ring RAD21, SMC1A, and SMC3. Notably, a physical interaction between centromeric RNAs and RAD21, SMC1A, and SMC3 had not been detected before. However, recent research has spotted a connection between cohesin and transcription. A study found that centromeric transcription strengthens centromeric cohesion [46]. Accordingly, such increased centromeric cohesion could delay mitotic progression, explaining the phenotypes that we observed in the proteasome inhibitor treatments and the partial rescue obtained by the addition of α -amanitin. The interaction of α -Sat RNA with members of the cohesin ring could also explain the mitotic delay observed upon exogenous expression of these transcripts. However, this would imply that such ectopic RNAs bind to and act in the centromeres, which is technically challenging to prove.

On the other hand, the delayed mitotic onset resulting from targeted α -Sat RNA destruction that we observed could also be an effect of newly discovered links between transcription and cohesin loading. One recent study determined that the STAG1 and STAG2 cohesin subunits are loaded to dsDNA regions that contain RNA [47]. Accordingly, the degradation of α -Sat RNAs could hinder cohesin dynamics, altering proper mitotic progression.

In summary, we discovered a novel role of the proteasome in mitotic progression through the regulation of α -Sat RNA levels. We propose that this previously unsuspected mechanism contributes to the mitotic arrest imposed by proteasome inhibitors, possibly by promoting the formation of aberrant ribonucleoprotein complexes that affect the function of key mitotic factors, including cohesins. Furthermore, our findings open the door to new avenues of research focused on the association between proteasome dysfunction and the dysregulation of noncoding RNAs. Such investigation endeavor will help understand fundamental aspects of genome maintenance and cancer progression.

Materials and methods

Cell lines

The following cell lines were used: HCT-116 (colon cancer, ATCC CCL-247), SW480 (colon cancer, ATCC CCL-228),

BT-20 (breast cancer, ATCC HTB-19), Cal-51 (breast cancer, DSMZ ACC 302), MDA-MB-231 (breast cancer, ATCC HTB-26), and MDA-MB-157 (breast cancer, ATCC HTB-24). Cells were grown at 37 °C in a humidified atmosphere containing 5% CO₂ in 10% Fetal Bovine Serum (FBS)-supplemented McCoy's 5A (HCT-116 cells), EMEM (BT-20 cells), or DMEM medium (Cal-51, MDA-MB-231, and MDA-MB-157) (Gibco, Waltham, MA, USA). HEK293 (ATCC PCS-200-010) primary neonatal foreskin keratinocytes were cultured in *Dermal Cell Basal Medium* (ATCC PCS-200-030) without FBS but supplemented with a *Keratinocyte Growth kit* (ATCC PCS-200-040).

Vectors

Total RNA from SW-480 cells was reverse transcribed, amplified by PCR using primers against global α -Sat [12], and cloned into the pTZ57R/T vector using the InsTAclone PCR Cloning Kit (Thermo Scientific, K1214), according to the manufacturer's instructions. Sanger sequencing was performed to detect clones of interest, and α -Sat sequences were subcloned into the mammalian expression pCDNA3.1 (+) backbone (Thermo Scientific, V79109), using EcoRI digestion. Plasmids were rescreened and selected by Sanger sequencing. We obtained three different α -Sat expression constructs: 1R, consisting of one α -Sat monomer in 5'-3' orientation (CGSW3 sequence); 5R, consisting of five α -Sat monomers in 5'-3' orientation (CGSW2 sequence), and 10R, consisting of two consecutive CGSW2 in 3'-5' orientation, i.e., ten consecutive α -Sat monomers. The CGSW2 and CGSW3 sequences are available in GenBank (see [Data accessibility](#)). The insert of the MS2 vector was obtained from the plasmid pCR4-24XMS2SL stable, which was a gift from Robert Singer (Addgene plasmid # 31865; <http://n2t.net/addgene:31865>; [RRID: Addgene_31865](#)). This insert, consisting of 24 consecutive MS2 repeats [48], was subcloned into the pCDNA3.1(+) vector using EcoRI.

Chromatin immunoprecipitation (ChIP)

A total of 1.3×10^4 cells *per cm*² were seeded on 150 *cm*² dishes. After drug treatment, cells were harvested, counted, and fixed in PBS containing 1% formaldehyde for 10 min. Fixation was quenched with 125 mM glycine for 10 min, and the cells were lysed in 50 mM Tris-HCl, 85 mM KCl, 10 mM EDTA, 1% SDS, and 1× protease inhibitor cocktail (Cell Signaling Technology #5876, Danvers, MA, USA) after two PBS washes. From this point on, ChIP assays were performed with the OneDay ChIP kit (Diagenode Kch-onedIP-180, Denville, NJ, USA) according to the manufacturer's instructions. One and a half million cells were used for each ChIP assay, using Magna ChIP™ Protein A + G Magnetic Beads (Millipore, 16-663, Darmstadt, Germany), followed by quantitative PCR (qPCR) amplification of candidate chromatin loci. For each qPCR, the amplification efficiency

(AE) of primers was calculated from serially diluted INPUT (10%, 5%, 1%, and 0.1%). The % of INPUT in each IP sample was calculated using the AE of the corresponding INPUT and normalized against the background ChIP experiment using control IgG. The qPCR amplifications were performed using Thermo Maxima SYBR Green/ROX 1 PCR Master Mix (Thermo Scientific, K0222) in a Step One Plus Real-Time PCR system (Applied Biosystems, 4376600, Waltham, MA, USA).

Nuclear extracts

Cells were lysed first in hypotonic buffer (10× the pellet volume): 10 mM Tris (pH 7.9), 10 mM KCl, 1.5 mM MgCl₂, 0.5% NP40, 40 mM β -glycerophosphate, 0.2 mM Na₃VO₄, 10 mM PNPP, 2 mM DTT, 1× Protease Inhibitor Cocktail (Roche, Darmstadt, Germany), and 10 nM PMSF for 30 min at 4 °C. Nuclei were then centrifuged at 4 °C for 1 min at 600 *g*, and the pellet was washed once with 1 mL of hypotonic buffer. Nuclear extracts were recovered through the addition of RIPA lysis buffer and centrifugation at full speed for 10 min at 4 °C. Nuclear extracts were resuspended in 150 mM KCl, 10% glycerol, 10 mM HEPES, 1 mM EDTA, 0.5% Triton X-100, 15 μ g·mL⁻¹ tRNA, 1 mM DTT, and 240 U RNase.

RNA pull-down

We determined a consensus sequence between the different α -Sat monomers in our 5R plasmid consisting of five α -Sat monomers in a sense orientation [24] (Fig. S3B). Biotinylated oligonucleotides were designed based on the resulting consensus sequence (see *Oligonucleotide table*). The RNA pull-down method has been described elsewhere [15], and a diagram of the procedure is shown in Fig. S3A. Briefly, we performed *in vitro* transcription from the 5R construct linearized downstream of the five repeats, and incubated 400 pmol of denatured RNA with 500 pmol of biotinylated probe in 50 mM KCl supplemented with 120 U of RNaseOUT™ (Invitrogen, 10777019, Carlsbad, CA, USA) for 1 h at RT. The RNA:probe complex was then incubated with magnetic streptavidin beads (2.5 mg) in 100 mM KCl, 5% glycerol, 5 mM HEPES, 0.5 mM EDTA, 0.25% Triton X-100, and 120 U RNaseOUT™ for an additional 30 min at RT. RNA:probe:bead complexes were washed two times in 50 mM KCl and then incubated with 4 mg of nuclear extract in 2 mL for 2 h at 4 °C. After two washes in the same buffer, the bound proteins were resuspended in Laemmli buffer, separated in a precast gel (Invitrogen), and sent for mass spectrometry analysis (Taplin Biological Mass Spectrometry Facility, Harvard Medical School, Boston). As a control, and to exclude nonspecific interactions between RNA and proteins, we performed the same experiment in parallel using a noncoding RNA fragment of the same size transcribed *in vitro* from a fragment of the luciferase

cDNA, using a complementary biotinylated probe. The data were analyzed using the STRING protein software [22].

Cell cycle synchronization and treatments

Cells were seeded 24 h before the beginning of the experiments. We synchronized cells with a single, 16 h, 2 mM thymidine block (Sigma T1895, Darmstadt, Germany) to synchronize cells in G1. The cultures were subsequently released in fresh medium for 4 h, at which they reached S-phase, or 7 h to reach G2/M phase. The concentration of the other drugs used was as follows: 100 nM Taxol (Sigma 7191), 2 $\mu\text{g}\cdot\text{mL}^{-1}$ nocodazole (Sigma M1404), 50 $\mu\text{g}\cdot\text{mL}^{-1}$ α -amanitin (Sigma A2263), 20 μM MG132 (Sigma C2211), 30 μM proTAME (Boston Biochem, I-440, Cambridge, MA, USA), and 100 nM bortezomib (Selleckchem, S1013, Houston, TX, USA).

Flow cytometric analysis

A total of 1.3×10^4 cells *per* cm^2 were seeded on six-well plates and synchronized in G2 phase as described above. After treatment, the cells were washed in PBS, trypsinized, fixed in 70% cold ethanol, and incubated at -20°C for at least 12 h. The cells were then washed once and resuspended in PBS and stained with 10 $\mu\text{g}\cdot\text{mL}^{-1}$ propidium iodide in 1.1% sodium citrate buffer supplemented with 0.25 $\text{mg}\cdot\text{mL}^{-1}$ RNase A for 2 h in the dark. Data were collected with a FACSCanto II flow cytometer (Becton Dickinson, San Jose, CA, USA) and analyzed with FACSDIVA 6.1.3 software (Becton Dickinson). The distribution of the DNA content was analyzed with FACSDIVA software. Cell cycle phases were determined using MODFIT LT 4.0 software (Becton Dickinson).

Immunofluorescence

A total of 1.3×10^4 cells *per* cm^2 were seeded on 22×22 mm glass coverslips 24 h before the beginning of the experiments. Cells were washed in PBS and fixed with 1% formaldehyde or cold methanol and permeabilized with acetone. The cells were then washed three times in PBS and blocked with 1% BSA for 1 h at RT. Cells were separately incubated with primary and secondary antibodies diluted in 1% BSA for 1 h at 37°C in a humid chamber, followed by three PBS washes. The coverslips were mounted on glass slides with Vectashield mounting medium containing DAPI (Vector Laboratories H-1200, Burlingame, CA, USA). Images were captured with an ELYRA (Zeiss, Jena, Germany) microscope.

Mitotic index determination

Mitotic indices were determined as described elsewhere [49]. Briefly, the cells were incubated in a hypotonic solution (10 mM HEPES – 262 nM EGTA – 40 mM KCl) for 30 min at 37°C , harvested with a scraper, and fixed in an ice-cold

methanol/acetic acid (3:1) fixation solution. The cells were then mounted onto slides and stained with eosin/methylene blue. The mitotic index was determined by observing the slides under a light microscope to determine mitotic figures. At least 1000 cells were counted per slide.

Northern blotting

RNA was extracted with TRIzol (Ambion, 15596018, Vilnius, Lithuania) according to the manufacturer's instructions. Twenty micrograms of total RNA from each cell condition were used for Northern blot analysis using a NorthernMax[®] Kit (Applied Biosystems AM1940) according to the manufacturer's instructions. After gel electrophoresis, RNAs were transferred to a Hybond-N+ nylon membrane (Amersham Hybond, GE Healthcare, Chicago, IL, USA) and hybridized with dCTP[³²P]-labeled DNA probes specific to α -Sat sequences (see *Oligonucleotide table* in Appendix S1).

RT-qPCR

A total of 1.3×10^4 cells *per* cm^2 were seeded on six-well plates, 24 h before the beginning of experiments. After treatment, cells were washed with PBS, and RNA was extracted with TRIzol (Ambion, 15596018) according to the manufacturer's instructions. Contaminant DNA was digested with a TURBO DNA-Free kit (Ambion, AM1907) according to the manufacturer's instructions. RNA integrity was assessed in a TapeStation apparatus (Agilent Technologies, Santa Clara, CA, USA), and cDNA was synthesized using a High-Capacity cDNA Reverse Transcription kit (Applied Biosystems, 4368814). qPCR was performed in a Step One Plus Real-Time Thermal Cycler (Applied Biosystems, 4376600) using a Maxima SYBR Green/ROX qPCR Master Mix 2 \times kit (Thermo Scientific, K0221).

Plasmid transfection

A total of 8.4×10^3 SW-480 cells were seeded *per* cm^2 on six-well plates and grown for 72 h. The cells in each well were transfected with 3.5 μg of plasmid with Lipofectamine 3000[™] (Thermo Fisher Scientific, 3000015) according to the manufacturer's instructions. Cells were harvested 48 h post-transfection, and duplicate wells treated in parallel were processed for flow cytometry or RT-qPCR.

ASO transfection

A total of 4×10^4 cells *per* cm^2 were seeded in 12-well plates and cultured for 2 days. The cells in each well were transfected with 250 pmol of ASO with Lipofectamine RNAiMAX[™] (Invitrogen, 13778) according to the manufacturer's instructions. Cells were harvested 24 h after transfection.

Western blot

A total of 1.3×10^4 cells *per* cm² were seeded on 10 cm dishes. After treatment, the cells were lysed in lysis buffer (#9803, Cell Signaling) supplemented with 100 μ M phenylmethylsulfonyl fluoride (PMSF) and collected with a scraper. The samples were centrifuged for 30 min at 19 000 *g* at 4 °C, and the supernatants were collected. Proteins (10–30 μ g) were separated on 10–12% SDS-polyacrylamide gels by electrophoresis and then transferred to polyvinylidene difluoride (PVDF) membranes (Immobilon-P, Millipore Corp.). The membranes were blocked in 3% BSA (in TBS-Tween) and incubated overnight with the indicated antibodies. To detect proteins, we used mouse IgG κ light-chain binding protein conjugated to HRP (m-IgG κ BP-HRP, Santa Cruz Biotechnology, sc-516102, Santa Cruz, CA, USA) and Immobilon Western Chemiluminescent HRP Substrate (WBKLS0100, Millipore). Densitometric analyses were performed with IMAGEJ software (National Institutes of Health, Bethesda, MD, USA).

RNA-seq and data analysis

Twenty RNA-Seq samples (four biological replicates of five conditions) were pooled and sequenced on NovaSeq_SP using Illumina TruSeq Stranded Total RNA Library Prep and paired-end sequencing. Raw sequencing reads were checked for quality with fastqc, adapter removal and quality trimming were performed with cutadapt version 1.18 with parameters --nextseq-trim=2 --trim-n -n 5 -O 5 -q 10,10 -m 35:35. We obtained 78–113 million that passed filter reads with more than 91% of bases above the quality score of Q30. Mapping to the human genome (assembly hg38) was performed with STAR ALIGNER [50,51] version 2.7.1a with special parameters winAnchorMultimapNmax 200--outFilterMultimapNmax 100 for multimapping reads. Gene and subfamily repetitive elements quantification was performed with TEcount (version 2.1.3), part of the TEtranscripts package [50,52], using GENCODE v34 annotations for genes and the provided curated repeat annotations for hg38 found in (http://labshare.cshl.edu/shares/mhammellab/www-data/TEtranscripts/TE_GTF/). Differential expression analysis was performed with DESeq2 [53], where DE genes and repeat subfamilies were defined with a cutoff of \log_2 FoldChange $> \log_2(1.5)$ and P adj < 0.05 . Gene ontology analysis was performed using the package clusterProfiler from Bioconductor [54]. Alpha Sat sequences CGSW2 and CGSW3 (see *Vectors*) were quantified using SALMONTE [52] version 0.4 with the default parameters to get gene counts by building an index that incorporated the α -Sat sequences to the provided *Homo sapiens* repeat annotation file (found in <https://github.com/LiuzLab/SalmonTE/blob/master/scripts>). Karyotype plots were produced with the package karyplotR from Bioconductor [55], where the density of repeat instances was computed on 500KB windows over the whole genome.

Three-dimensional immuno-FISH

A total of 1.3×10^4 cells *per* cm² were seeded on 18 mm \times 18 mm, 0.17 mm thick glass coverslips (Zeiss). After treatment, the cells were fixed in 4% PFA for 20 min. After three PBS washes, the cells were permeabilized in ice-cold 0.4% Triton-X-100/PBS for 20 min on ice and incubated in blocking solution for 1 h (2.5% bovine serum albumin (BSA), 10% Normal Goat Serum, and 0.1% Tween-20). The cells were incubated with the primary antibodies overnight at 4 °C in a humid chamber. Then, the cells were washed with 0.2% BSA/0.1% Tween-20/PBS three times for 5 min at RT and subsequently incubated with the secondary antibody Dylight 405 (Goat anti-Mouse, Thermo Fisher Cat. No. 35501BID) diluted in blocking solution for 1 h at RT in a dark and humid chamber. Cells were washed three times in 0.1% Tween-20/PBS for 5 min in a rocking plate in the dark. Postfixation was performed in 2% PFA for 10 min followed by three PBS washes. Cells were incubated with RNase A for 1 h at 37 °C and washed three times in PBS. A permeabilization step was performed in ice-cold 0.7% Triton-X-100/0.1 M HCl for 10 min on ice. The cells were denatured in 1.9 M HCl and then washed once with 2X SSC. Then, 10 μ L of the Star*-FISHTM pancentromeric FISH probe were added to each coverslip (Cambio, 1695-F, Cambridge, UK). After overnight incubation in a humid chamber at 37 °C, the cells were washed with 2x SSC for 30 min at 37 °C, 2xSSC for 30 min at RT, and 1xSSC for 30 min at RT in the dark on a rocking plate. Finally, coverslips were mounted on slides with 10 μ L of Vectaschield (Vector Laboratories H-1200) and sealed.

Microscope and image acquisition

Super-resolution imaging (3D-SIM) was performed on a Zeiss Elyra PS1 equipped with a Zeiss Plan Apochromat inverted 100 \times /1.46 oil immersion objective lens using an Andor EM-CCD. The blue channel was obtained with 405 nm laser excitation, 23 mm diffraction grating, and filter cube SR Cube 07. The Cy3 channel was obtained with 561 nm laser excitation. The FITC channel was obtained with 488 nm laser excitation. The lateral pixel size, D_x and D_y , was 79 nm in the recorded images and 40 nm in the reconstructed image. The z-stacks were acquired by capturing slices taken at 83 nm intervals through each nucleus and consisted of 70–90 slices collected sequentially. A field of view was selected, and the z-stack boundaries were defined manually. The 3D-SIM images were reconstructed using IMARIS (V.9.0.2, Bitplane). The full 3D image was used for analysis, and colocalization analyses were based on Pearson's correlation (PC) coefficient, assessing the correlation of data sets in a voxel-by-voxel intensity-based analysis.

Acknowledgements

Rodrigo E. Cáceres-Gutiérrez is a doctoral student from Programa de Doctorado en Ciencias Biomédicas, Universidad Nacional Autónoma de México (UNAM) and received CONACYT fellowship 290129; and was supported by Programa de Apoyo a Estudiantes de Posgrado, UNAM, for a research stay in Dr Francastel's laboratory. We thank Dr Alain Sureau for his assistance with Northern blotting; Dr Guillaume Velasco for helpful discussions; and Iyonne Elizabeth Arriaga Guzmán, José de Jesús Naveja, Sebastián Mohar, Valeria P. Molina, Jaime Barrera, Luis F. González, Fabiola G. Flores, and María F. Ruíz for technical assistance. We sincerely thank all members of the CCR Sequencing Facility at the Frederick National Laboratory for Cancer Research for their help during sample preparation and sequencing. We thank the Unidad de Microscopía Avanzada INCANRAI-UNAM at the Instituto Nacional de Cancerología, México, for their help in image capture and analysis.

Conflict of interest

The authors declare no conflict of interest.

Author contributions

Project design: REC-G & LAH; RNA-seq performance and analysis: REC-G, EIN, BT, JS, YZ, and NA; experimental design & result analysis: REC-G, MAA, DAO, RGB, FL, CAC, AL, CC, JD, YA, EF, SH, FH, CF, and LAH; performed experiments: REC-G, MAA, DAO, RGB, FL, CAC, AL, CC, JD, YA, EF, CDR, JLR, and FH; statistical analysis: DP; manuscript writing: REC-G; manuscript revision: CF & LAH; project supervision: CF & LAH, software development: REC-G & LP; funding acquisition: LAH.

Peer Review

The peer review history for this article is available at <https://publons.com/publon/10.1111/febs.16261>.

Data accessibility

Flow cytometry data are available in the FlowRepository database: <https://flowrepository.org/> under the following IDs: FR-FCM-Z3G4, FR-FCM-Z3FE, and FR-FCM-Z3GY. Novel nucleic acid sequences: CGSW2, GenBank accession number MW491379, and CGSW3, GenBank accession number: MW491380.

RNA-seq data are available in GEO: <https://www.ncbi.nlm.nih.gov/geo/query/acc.cgi?acc=GSE165325>. The mass spectrometry proteomics data have been deposited to the ProteomeXchange Consortium via the PRIDE partner repository with the dataset identifiers PXD024582 and 10.6019/PXD024582. The Morgan Hunter tool is available on GitHub: <https://github.com/laurentp89/morgan-hunter>

References

- Geng F, Wenzel S & Tansey WP (2012) Ubiquitin and proteasomes in transcription. *Annu Rev Biochem* **81**, 177–201.
- Fricker LD (2020) Proteasome inhibitor drugs. *Annu Rev Pharmacol Toxicol* **60**, 457–476.
- Frankland-Searby S & Bhaumik SR (2012) The 26S proteasome complex: an attractive target for cancer therapy. *Biochim Biophys Acta* **1825**, 64–76.
- Musacchio A & Salmon ED (2007) The spindle-assembly checkpoint in space and time. *Nat Rev Mol Cell Biol* **8**, 379–393.
- Zeng X, Sigoillot F, Gaur S, Choi S, Pfaff KL, Oh D-C, Hathaway N, Dimova N, Cuny GD & King RW (2010) Pharmacologic inhibition of the anaphase-promoting complex induces a spindle checkpoint-dependent mitotic arrest in the absence of spindle damage. *Cancer Cell* **18**, 382–395.
- Kito Y, Matsumoto M, Hatano A, Takami T, Oshikawa K, Matsumoto A & Nakayama KI (2020) Cell cycle-dependent localization of the proteasome to chromatin. *Sci Rep* **10**, 5801.
- Natisvili T, Yandim C, Silva R, Emanuelli G, Krueger F, Nageswaran S & Festenstein R (2016) Transcriptional activation of pericentromeric satellite repeats and disruption of centromeric clustering upon proteasome inhibition. *PLoS One* **11**, e0165873.
- Chan FL & Wong LH (2012) Transcription in the maintenance of centromere chromatin identity. *Nucleic Acids Res* **40**, 11178–11188.
- Fukagawa T & Earnshaw WC (2014) The centromere: chromatin foundation for the kinetochore machinery. *Dev Cell* **30**, 496–508.
- McNulty SM & Sullivan BA (2018) Alpha satellite DNA biology: finding function in the recesses of the genome. *Chromosome Res* **26**, 115–138.
- Henikoff S, Ahmad K & Malik HS (2001) The centromere paradox: stable inheritance with rapidly evolving DNA. *Science* **293**, 1098–1102.
- Chan FL, Marshall OJ, Saffery R, Kim BW, Earle E, Choo KHA & Wong LH (2012) Active transcription and essential role of RNA polymerase II at the centromere during mitosis. *Proc Natl Acad Sci USA* **109**, 1979–1984.

- 13 Quénet D & Dalal Y (2014) A long non-coding RNA is required for targeting centromeric protein A to the human centromere. *eLife* **3**, e03254.
- 14 McNulty SM, Sullivan LL & Sullivan BA (2017) Human centromeres produce chromosome-specific and array-specific alpha satellite transcripts that are complexed with CENP-A and CENP-C. *Dev Cell* **42**, 226–240.e6.
- 15 Ferri F, Bouzinba-Segard H, Velasco G, Hubé F & Francastel C (2009) Non-coding murine centromeric transcripts associate with and potentiate Aurora B kinase. *Nucleic Acids Res* **37**, 5071–5080.
- 16 Bury L, Moodie B, Ly J, McKay LS, Miga KH & Cheeseman IM (2020) Alpha-satellite RNA transcripts are repressed by centromere-nucleolus associations. *eLife* **9**, e59770.
- 17 Jambhekar A, Emerman AB, Schweidenback CTH & Blower MD (2014) RNA stimulates Aurora B kinase activity during mitosis. *PLoS One* **9**, e100748.
- 18 Eymery A, Horard B, El Atifi-Borel M, Fourel G, Berger F, Vitte A-L, Van den Broeck A, Brambilla E, Fournier A, Callanan M *et al.* (2009) A transcriptomic analysis of human centromeric and pericentric sequences in normal and tumor cells. *Nucleic Acids Res* **37**, 6340–6354.
- 19 Valgardsdottir R, Chiodi I, Giordano M, Rossi A, Bazzini S, Ghigna C, Riva S & Biamonti G (2008) Transcription of satellite III non-coding RNAs is a general stress response in human cells. *Nucleic Acids Res* **36**, 423–434.
- 20 Hédouin S, Grillo G, Ivkovic I, Velasco G & Francastel C (2017) CENP-A chromatin disassembly in stressed and senescent murine cells. *Sci Rep* **7**, 42520.
- 21 Gao XD, Tu L-C, Mir A, Rodriguez T, Ding Y, Leszyk J, Dekker J, Shaffer SA, Zhu LJ, Wolfe SA *et al.* (2018) C-BERST: defining subnuclear proteomic landscapes at genomic elements with dCas9-APEX2. *Nat Methods* **15**, 433–436.
- 22 Szklarczyk D, Gable AL, Lyon D, Junge A, Wyder S, Huerta-Cepas J, Simonovic M, Doncheva NT, Morris JH, Bork P *et al.* (2019) STRING v11: protein-protein association networks with increased coverage, supporting functional discovery in genome-wide experimental datasets. *Nucleic Acids Res* **47**, D607–D613.
- 23 Agostini F, Zanzoni A, Klus P, Marchese D, Cirillo D & Tartaglia GG (2013) catRAPID omics: a web server for large-scale prediction of protein-RNA interactions. *Bioinformatics* **29**, 2928–2930.
- 24 Wu JC & Manuelidis L (1980) Sequence definition and organization of a human repeated DNA. *J Mol Biol* **142**, 363–386.
- 25 Ugarkovic D (2005) Functional elements residing within satellite DNAs. *EMBO Rep* **6**, 1035–1039.
- 26 Wayne JS & Willard HF (1987) Nucleotide sequence heterogeneity of alpha satellite repetitive DNA: a survey of alphoid sequences from different human chromosomes. *Nucleic Acids Res* **15**, 7549–7569.
- 27 Johnson M, Zaretskaya I, Raytselis Y, Merezhuk Y, McGinnis S & Madden TL (2008) NCBI BLAST: a better web interface. *Nucleic Acids Res* **36**, W5–W9.
- 28 Bucher P (1990) Weight matrix descriptions of four eukaryotic RNA polymerase II promoter elements derived from 502 unrelated promoter sequences. *J Mol Biol* **212**, 563–578.
- 29 Dreos R, Ambrosini G, Périer RC & Bucher P (2015) The Eukaryotic Promoter Database: expansion of EPDnew and new promoter analysis tools. *Nucleic Acids Res* **43**, D92–D96.
- 30 Mantovani R (1998) A survey of 178 NF-Y binding CCAAT boxes. *Nucleic Acids Res* **26**, 1135–1143.
- 31 Dolfini D, Zambelli F, Pavesi G & Mantovani R (2009) A perspective of promoter architecture from the CCAAT box. *Cell Cycle* **8**, 4127–4137.
- 32 Zerbino DR, Achuthan P, Akanni W, Amode MR, Barrell D, Bhai J, Billis K, Cummins C, Gall A, Girón CG *et al.* (2018) Ensembl 2018. *Nucleic Acids Res* **46**, D754–D761.
- 33 Salsi V, Caretti G, Wasner M, Reinhard W, Haugwitz U, Engeland K & Mantovani R (2003) Interactions between p300 and multiple NF-Y trimers govern cyclin B2 promoter function. *J Biol Chem* **278**, 6642–6650.
- 34 Fleming JD, Pavesi G, Benatti P, Imbriano C, Mantovani R & Struhl K (2013) NF-Y coassociates with FOS at promoters, enhancers, repetitive elements, and inactive chromatin regions, and is stereo-positioned with growth-controlling transcription factors. *Genome Res* **23**, 1195–1209.
- 35 Kinyamu HK, Bennett BD, Bushel PR & Archer TK (2020) Proteasome inhibition creates a chromatin landscape favorable to RNA Pol II processivity. *J Biol Chem* **295**, 1271–1287.
- 36 Poulaki V, Mitsiades CS, Kotoula V, Negri J, McMillin D, Miller JW & Mitsiades N (2007) The proteasome inhibitor bortezomib induces apoptosis in human retinoblastoma cell lines in vitro. *Invest Ophthalmol vis Sci* **48**, 4706–4719.
- 37 Daum JR, Potapova TA, Sivakumar S, Daniel JJ, Flynn JN, Rankin S & Gorbsky GJ (2011) Cohesion fatigue induces chromatid separation in cells delayed at metaphase. *Curr Biol* **21**, 1018–1024.
- 38 Ohzeki J, Bergmann JH, Kouprina N, Noskov VN, Nakano M, Kimura H, Earnshaw WC, Larionov V & Masumoto H (2012) Breaking the HAC Barrier: histone H3K9 acetyl/methyl balance regulates CENP-A assembly. *EMBO J* **31**, 2391–2402.
- 39 Ishikura S, Nakabayashi K, Nagai M, Tsunoda T & Shirasawa S (2020) ZFAT binds to centromeres to control noncoding RNA transcription through the

- KAT2B-H4K8ac-BRD4 axis. *Nucleic Acids Res* **48**, 10848–10866.
- 40 Jang MK, Mochizuki K, Zhou M, Jeong H-S, Brady JN & Ozato K (2005) The bromodomain protein Brd4 is a positive regulatory component of P-TEFb and stimulates RNA polymerase II-dependent transcription. *Mol Cell* **19**, 523–534.
- 41 Oldfield AJ, Yang P, Conway AE, Cinghu S, Freudenberg JM, Yellaboina S & Jothi R (2014) Histone-fold domain protein NF-Y promotes chromatin accessibility for cell type-specific master transcription factors. *Mol Cell* **55**, 708–722.
- 42 Tsukamoto S & Yokosawa H (2009) Targeting the proteasome pathway. *Expert Opin Ther Targets* **13**, 605–621.
- 43 Bensauade O (2011) Inhibiting eukaryotic transcription: Which compound to choose? How to evaluate its activity? *Transcription* **2**, 103–108.
- 44 Benatti P, Dolfini D, Viganò A, Ravo M, Weisz A & Imbriano C (2011) Specific inhibition of NF-Y subunits triggers different cell proliferation defects. *Nucleic Acids Res* **39**, 5356–5368.
- 45 Johnson WL, Yewdell WT, Bell JC, McNulty SM, Duda Z, O'Neill RJ, Sullivan BA & Straight AF (2017) RNA-dependent stabilization of SUV39H1 at constitutive heterochromatin. *eLife* **6**, e25299.
- 46 Chen Y, Zhang Q, Teng Z & Liu H (2021) Centromeric transcription maintains centromeric cohesion in human cells. *J Cell Biol* **220**, e202008146.
- 47 Pan H, Jin M, Ghadiyaram A, Kaur P, Miller HE, Ta HM, Liu M, Fan Y, Mahn C, Gorthi A *et al.* (2020) Cohesin SA1 and SA2 are RNA binding proteins that localize to RNA containing regions on DNA. *Nucleic Acids Res* **48**, 5639–5655.
- 48 Bertrand E, Chartrand P, Schaefer M, Shenoy SM, Singer RH & Long RM (1998) Localization of ASH1 mRNA particles in living yeast. *Mol Cell* **2**, 437–445.
- 49 Polito P, Dal Cin P, Debiec-Rychter M & Hagemeyer A (2003) Human solid tumors: cytogenetic techniques. *Methods Mol Biol* **220**, 135–150.
- 50 Jin Y, Tam OH, Paniagua E & Hammell M (2015) TETranscripts: a package for including transposable elements in differential expression analysis of RNA-seq datasets. *Bioinformatics* **31**, 3593–3599.
- 51 Dobin A, Davis CA, Schlesinger F, Drenkow J, Zaleski C, Jha S, Batut P, Chaisson M & Gingeras TR (2013) STAR: ultrafast universal RNA-seq aligner. *Bioinformatics* **29**, 15–21.
- 52 Jeong H-H, Yalamanchili HK, Guo C, Shulman JM & Liu Z (2018) An ultra-fast and scalable quantification pipeline for transposable elements from next generation sequencing data. *Pac Symp Biocomput* **23**, 168–179.
- 53 Love MI, Huber W & Anders S (2014) Moderated estimation of fold change and dispersion for RNA-seq data with DESeq2. *Genome Biol* **15**, 550.
- 54 Yu G, Wang L-G, Han Y & He Q-Y (2012) clusterProfiler: an R package for comparing biological themes among gene clusters. *OMICS* **16**, 284–287.
- 55 Gel B & Serra E (2017) karyoploteR: an R/Bioconductor package to plot customizable genomes displaying arbitrary data. *Bioinformatics* **33**, 3088–3090.

Supporting information

Additional supporting information may be found online in the Supporting Information section at the end of the article.

Fig. S1. Transcripts differentially expressed under MG132 and bortezomib treatment.

Fig. S2. Proteasome inhibition-dependent α -Sat RNA upregulation can occur in mitosis and is independent of APC/C in HCT-116 cells.

Fig. S3. RNA pull-down procedure.

Fig. S4. Experimental alteration of α -Sat RNA abundance.

Fig. S5. α -Sat transcript levels vary with cell type.

Fig. S6. α -Sat DNA bears CCAAT boxes and is bound by NFY-A.

Table S1. Proteins enriched in α -Sat RNA fraction.

Appendix S1. Materials and methods.

Dataset S1. Location of differentially expressed repeat transcript subfamilies in MG132 (pink) and bortezomib (lavender) along each chromosome, entire dataset. Instances are condensed in 500 kb windows.

Dataset S2. Mapping of each clone to the Hg38 using the ENSEMBL BLAT tool.

Dataset S3. Location of CCAAT-box-bearing α -satellite monomers (grey histograms), TATA-box-bearing α -satellite monomers (black histograms) and the α -satellite RNAs differentially expressed under MG132 and bortezomib (red histograms), along each chromosome. Entire dataset.